The Phylogeography of Deciduous Tree *Ulmus macrocarpa* (Ulmaceae) in Northern China

Hang Ye [1,†] **, Yiling Wang** [2,*] **, Hengzhao Liu** [1,†] **, Dingfan Lei** [1] **, Haochen Li** [1] **, Zhimei Gao** [1] **, Xiaolong Feng** [2] **, Mian Han** [2] **, Qiyang Qie** [2] **and Huijuan Zhou** [3,*]

1. Key Laboratory of Resource Biology and Biotechnology in Western China, Ministry of Education, College of Life Sciences, Northwest University, Xi'an 710069, China; phdye@stumail.nwu.edu.cn (H.Y.); hengzhaoliu@stumail.nwu.edu.cn (H.L.); leidingfan@stumail.nwu.edu.cn (D.L.); lihaochen@stumail.nwu.edu.cn (H.L.); gaozhimei@stumail.nwu.edu.cn (Z.G.)
2. School of Life Sciences, Shanxi Normal University, Taiyuan 030031, China; 221112089@sxnu.edu.cn (X.F.); 222112039@sxnu.edu.cn (M.H.); 221112090@sxnu.edu.cn (Q.Q.)
3. Xi'an Botanical Garden of Shaanxi Province (Institute of Botany of Shaanxi Province), Xi'an 710061, China
* Correspondence: 309023@sxnu.edu.cn (Y.W.); zhouhuijuan@xab.ac.cn (H.Z.)
† These authors contributed equally to this work.

Abstract: Disentangling how climate oscillations and geographical events significantly influence plants' genetic architecture and demographic history is a central topic in phytogeography. The deciduous ancient tree species *Ulmus macrocarpa* is primarily distributed throughout Northern China and has timber and horticultural value. In the current study, we studied the phylogenic architecture and demographical history of *U. macrocarpa* using chloroplast DNA with ecological niche modeling. The results indicated that the populations' genetic differentiation coefficient (N_{ST}) value was significantly greater than the haplotype frequency (G_{ST}) ($p < 0.05$), suggesting that *U. macrocarpa* had a clear phylogeographical structure. Phylogenetic inference showed that the putative chloroplast haplotypes could be divided into three groups, in which the group I was considered to be ancestral. Despite significant genetic differentiation among these groups, gene flow was detected. The common ancestor of all haplotypes was inferred to originate in the middle–late Miocene, followed by the haplotype overwhelming diversification that occurred in the Quaternary. Combined with demography pattern and ecological niche modeling, we speculated that the surrounding areas of Shanxi and Inner Mongolia were potential refugia for *U. macrocarpa* during the glacial period in Northern China. Our results illuminated the demography pattern of *U. macrocarpa* and provided clues and references for further population genetics investigations of precious tree species distributed in Northern China.

Keywords: *Ulmus macrocarpa*; phytogeography; climate oscillations; Northern China; refugia

1. Introduction

Inferring the spatio-temporal diversity patterns and demography history of species has been central in phytogeography since its conception. Climatic-induced environmental alterations, coupled with geological phenomena, exert a significant influence on the geographical distribution of species and the dynamics of population demographics [1], especially in ancient tree species with relatively long evolutionary histories [2–4]. Being a vital vegetation type in the Northern Hemisphere, the origin and historical biogeography of temperate forest biome have received extensive attention since the nineteenth century [5–7]. Nevertheless, our comprehension of this subject remains constrained.

Climatic oscillations during Quaternary periods with more frequent glacial–interglacial cycles dramatically affected the species diversity pattern in Northern Hemisphere [8–10]. Within the realm of East Asia, it is posited that a minimum of four notable glaciations have taken place, presumably impacting the region's flora and fauna, albeit the glacial

progressions were less encompassing compared to Europe and North America [1,11,12]. Specifically, Northern China underwent drastic climatic fluctuations throughout the Quaternary period, yet it was never blanketed by extensive ice sheets [1,10,12]. The suitable habitat during the glacial period served as species' refugia and played a critical role in species' post-glaciation recolonization [13,14]. Previous research has proposed distinct refugia patterns for woody species in China, including single refugia, multiple refugia, microrefugia, and cryptic refugia [13,15,16]. However, a significant bulk of studies have been primarily fixated on the populations or species in Southern, Southwestern, and Northwestern China [9,17,18], leaving the northern zones under-researched and less explored.

The Elm family (Ulmaceae) is a moderately sized family consisting of approximately 50–60 species in the order Rosales. In Ulmaceae, the genera *Ulmus*, *Hemiptelea*, and *Planera* are predominantly deciduous and widely distributed in the northern temperate zone. Hence, the exploration of Ulmaceae's biogeographic and demographic history could provide insights into the assembly of the temperate forest biome [19,20]. The previous study also emphasized the significance of Ulmaceae as a model system for investigating the boreal tree species' historical biogeography and diversification patterns [21]. It has been reported that Ulmaceae emerged in the Early Cretaceous and could be separated into a temperate clade and a tropical clade [20,21]. Coalescent simulation suggested an East Asian origin of the temperate Ulmaceae clade during the Paleocene, consistent with the fossil records [21]. The macroclimatic niche of Ulmaceae species varies between the tropical and temperate clades. Ecological preferences play a crucial role in determining the geographical distribution of Ulmaceae plants [20]. Elm species are adaptable and resist drought, cold, and saline–alkali stresses. Comparative transcriptome analysis showed that positively selective genes may play essential roles in adapting to environmental changes for elms [22].

Serving as the diversity center, China has the highest Ulmaceae diversity worldwide [20]. *Ulmus macrocarpa*, mainly distributed across Northern China, is a precious woody germplasm resource and a key part of forest communities [23]. This tree can reach 20 m in height with a diameter of 40 cm at breast height. Its branches are light yellow–brown or pale reddish–brown; leaves are broad obovate or elliptic–obovate, 5–9 cm long, with a pointed tip. Winged fruits, 2.5–3.5 cm long, are hairy and have seeds in the middle. Flowering is in April–May; fruiting is in May–June, and leaves fall in October [24].

U. macrocarpa has important pharmaceutical, horticultural, and timber values [25–27]. Its wood is high-quality and commonly used in various applications. The seeds of *U. macrocarpa* have top-ranked weight, oil content, and decanoic acid among *Ulmus* species [24]. Its seed oil is utilized in food, industries, brewing, soy sauce production, and medicine. The bark also contains polysaccharides and mucilage for medicinal use. Additionally, the *U. macrocarpa* is a heliophyte with strong sprouting ability, capable of resisting cold and drought conditions.

As an important germplasm resource in Ulmaceae, although *U. macrocarpa* had significant economic value and high ecological adaptability, the advanced molecular phytogeography research on *U. macrocarpa* received less attention compared to other Ulmaceae species. A previous study observed high phenotypic variations in *U. macrocarpa* populations. The micromorphological features of the leaf epidermis in *U. macrocarpa* were influenced by environmental factors such as temperature and altitude [24]. However, the genetic diversity and differentiation of *U. macrocarpa* was still unknown. Furthermore, owing to a lack of nuclear genome data, such research on elms is singularly lagging behind other species, with existing research limited to morphology, allozyme markers, molecular markers, and transcriptomes [10,22,28–36]. The chloroplast genome was popularly utilized in plant population genetics, polymorphism investigations, ecological and evolutionary studies, and DNA barcoding owing to its characteristics of small genome size, relatively slow evolutionary rates, and maternal inheritance. Meanwhile, the application of chloroplast DNA contributed a lot to plant phytogeography. Although the chloroplast genome was relatively conserved, single nucleotide polymorphisms (SNPs) frequently occurred, providing valuable variation resources for intra- or interspecific phytogeography research.

Thanks to the rapid development of sequencing technology, the complete chloroplast genome of *U. macrocarpa* has been published [21], providing an excellent opportunity for genetic investigation. The *ycf1* was the most promising plastid DNA barcode of land plants, which was more variable than other chloroplast barcodes such as *matK* and *rbcL* [37–39]. So far, the chloroplast *ycf1* has been widely used in phylogenic and phytogeographic studies [40–44]. In this study, in addition to *ycf1*, three chloroplast intergenic spacer regions *rpl32–trnL* [45], *atpB–rbcL* [46], and *trnH–psbA* [47] were also used to investigate phytogeography of *U. macrocarpa* because of their stable amplification success and high variability. This study aimed to achieve the following: (1) reveal the genetic diversity and genetic differentiation landscape of *U. macrocarpa* populations; (2) unveil the impact of climate heterogeneity and geographical isolation on *U. macrocarpa* population genetic architecture; (3) explore the demographic history of *U. macrocarpa*; and (4) discuss its refugia pattern during the glacial period. Our results would illuminate the demographic history of valuable tree species *U. macrocarpa* and offer a theoretical foundation for further biodiversity investigation of the temperate forest biome in Northern China and even East Asia.

2. Materials and Methods

2.1. Sample Collection, DNA Extraction, and Sequencing

We sampled 110 individuals from 22 populations (5 individuals per population) throughout the geographical distribution of *U. macrocarpa* in Northern China (Figure 1; Table S1). All samples from each population were separated by a distance exceeding 20 m, and fresh leaves were gathered for DNA extraction. The genome DNA was extracted from fresh leaves using a modified CTAB method [48]. The primers of *ycf1*, *rpl32–trnL*, *atpB-rbcL*, and *trnH-psbA* (Table S2) were designed according to the complete chloroplast genome of *U. macrocarpa* (NCBI accession number: MT165937.1) [21] using Primer Premier software 5 [49]. The DNA quality was then assessed through ultraviolet spectrophotometry and 0.8% agarose gel electrophoresis, followed by storage at $-20\,^\circ\text{C}$ for subsequent use.

The PCR protocols were adapted from Liu et al. [36], with the reaction carried out in a 25 µL volume comprising 4 µL of template DNA (30 ng/µL), 1 µL of primers, 12.5 µL of 2× MasterMix, and 7.5 µL of ddH$_2$O. The PCR process included pre-denaturation (94 $^\circ$C for 5 min), denaturation (94 $^\circ$C for 1 min), annealing (55 $^\circ$C for 1 min), elongation (72 $^\circ$C for 1.5 min) for 35 cycles, and final elongation (72 $^\circ$C for 10 min). The PCR products were detected using 2% agarose gel electrophoresis and confirmed through automated gel imaging analysis before being sent to Sangon Biotech (Shanghai, China) for sequencing.

2.2. Haplotype Identification and Genetic Diversity Analysis

After sequencing, the chloroplast DNA fragments were aligned using MAFFT [50] and then pruned by GBLOCKS [51]. Using the DNASP 6 software [52], the chloroplast haplotype was identified, followed by the calculation of nucleotide diversity (π) and haplotype diversity (Hd). The PERMUT 2.0 program [53] was used to estimate the genetic parameters, including gene diversity (h_S), total gene diversity (h_T), geographical total haplotype diversity (V_T), and geographical average haplotype diversity (V_S). The presence of phylogeographic structure was assessed by testing whether N_{ST} (genetic differentiation takes into account distances among haplotypes) was significantly higher than G_{ST} (population differentiation that does not consider distances among haplotypes) with 1000 times permutation tests. To quantify and assess the distribution of genetic variation within and between populations, a hierarchical analysis of molecular variance (AMOVA) was implemented by using ARLEQUIN 3.5 software [54] with 1000 times permutations.
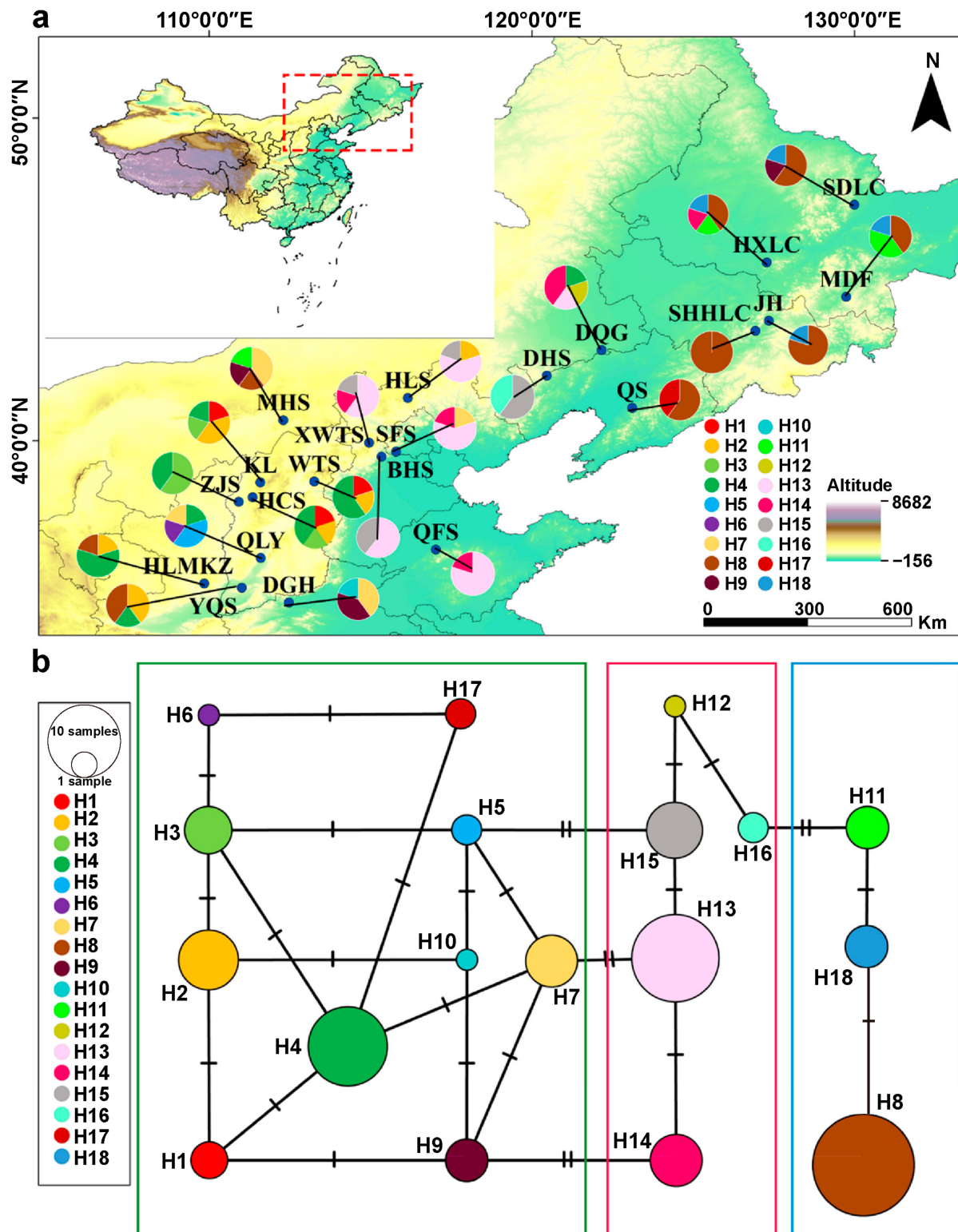
Figure 1. Sampling locations, haplotype distributions (**a**), and the network (**b**) of *U. macrocarpa* in Northern China. The pie chart represents the proportion of haplotypes in each population. Three frames in different colors (green, red, and blue) in network (**b**) correspond to the three different haplotype phylogenetic groups.

2.3. Phylogeny Inference and Genetic Structure Estimation

Different methods were employed to disentangle the genetic structure and phylogenetic relationship of *U. macrocarpa* populations. Nei's genetic distance was employed to

reconstruct a neighbor-joining (NJ) tree using POPTREE 2 [55] with 1000 times bootstrap replicates. A principal component analysis (PCA) of all studied populations was performed using GENALEX 6.5 [56].

Bayesian clustering analysis was executed using STRUCTURE 2.3 software [57]. The posterior probability of grouping number (K = 1–10) was estimated by conducting 10 independent runs using 5×10^5-step Markov chain Monte Carlo (MCMC) replicates, preceded by a 1×10^6-step burn-in for each run to assess consistency. The optimal grouping number was determined using ΔK method as calculated in STRUCTURE HARVESTER [58]. Subsequently, the results from these 10 runs were aligned and consolidated with CLUMPP 1.1.2 [59], and the visualization of the results was generated using DISTRUCT 1.1 [60]. When considering the sampling location, the genetic structure was assessed through a spatial analysis of molecular variance using SAMOVA 2.0 [61]. Similar to the STRUCTURE analysis, the number of groups (K) of geographically adjacent populations was set from 1 to 10 in SAMOVA. The geographical distance was employed as the prior condition for the population's genetic grouping, and the permutations test was set to 1000 times. The haplotype network was also constructed to reveal the phylogenetic relationship of putative haplotypes using POPART 1.7 [62].

To investigate the influence of isolation by geography and climate on the genetic differentiation of *U. macrocarpa* populations, the Mantel test and generalized linear model (GLM) were performed using the R package vegan [63]. Therein, pairwise FST values calculated from aligned sequences were utilized as a genetic distances matrix. The geographic distances matrix between populations was determined using GENALEX 6.5 software [56], and the environmental distances matrix was generated using PASSAGE 2 software [64].

2.4. Phylogeographical Pattern and Demographic History Inference

The BEAST 1.8.4 software [65] was used to estimate the haplotype divergence time of *U. macrocarpa*, in which *U. pulima* was employed as the outgroup. JMODELTEST 2 [66] was adopted to estimate the optimum substitution model according to the Akaike Information Criterion [67], and T92 was finally confirmed as the best-fit model. The evolutionary rates were set as 1.1 to 2.9×10^{-9} mutations per site per year, according to a previous study [68]. The fossil record for *U. macrocarpa* (20.44–15.97 Ma, https://paleobiodb.org/classic/basicTaxonInfo?taxon_no=445605 (accessed on 25 February 2024)) was used to time tree calibration [69]. With the relaxed clock model in lognormal distribution, the MCMC process was repeated 5×10^7 times by sampling every 20,000 generations to guarantee an effective sample size of over 200. We constructed a consensus tree with a posterior probability threshold exceeding 0.5 by utilizing TREE ANNOTATOR, following the exclusion of the initial 25% of trees as burn-in. The consensus tree was edited and visualized in FIGTREE.

To assess whether the species had experienced significant expansion, we used ARLEQUIN [54] to calculate the Tajima's D [70] and Fu's FS [71] values. Moreover, the sum of square deviation (SSD) and raggedness index (Rag) was also calculated in the mismatch distribution analysis (MDA) using ARLEQUIN. Phytogeography dynamics of *U. macrocarpa* were inferred via the Bayesian Binary MCMC (BBM) Method by using RASP 4 software [72]. Furthermore, the historical and contemporary gene flows during *U. macrocarpa* evolution were estimated by MIGRATE-N 3.7.2 [73] and BAYESASS 3 [74], respectively.

2.5. Ecological Niche Modeling

The maximum entropy modeling technique (MAXENT) [75] was utilized to predict the potential distribution of *U. macrocarpa* in China in different periods, including the contemporary period, mid-Holocene (MH, ~6 ka BP), Last Glacial Maximum (LGM, ~21 ka BP), and Last Interglacial (LIG, ~120–140 ka BP). In addition to the sampling sites in our study, the occurrence recodes of *U. macrocarpa* were also obtained from the Chinese Virtual Herbarium (CVH, http://www.cvh.ac.cn/ (accessed on 25 February 2024)) and

the National Specimen Information Infrastructure (NSII, http://www.nsii.org.cn). After filtering, 59 records were finally retained for ecological niche modeling (ENM).

A total of 19 biological climate variables (bio1–bio19) at 2.5 arc-min resolution were downloaded from the WorldClim database (http://www.worldclim.org (accessed on 25 February 2024)). To avoid overfitting caused by the multicollinearity of climate variables, the VIF (Variance Inflation Factor) method was employed for variable selection using the R package usdm [76]. Climate variables with VIF > 20 and high correlation ($|r| > 0.85$) were removed [77]. After filtering, five climate variables were retained, namely, bio3, bio6, bio8, bio14, and bio16. The receiver operating characteristic (ROC) curve was used to test the accuracy of the MAXENT prediction. The fitness of suitable habitats was manually divided into a gradient classification corresponding to unsuitable (0–0.1), lowly suitable (0.1–0.25), moderately suitable (0.25–0.5), and highly suitable regions (>0.5), respectively.

To investigate the overlaps and differentiation of the niches between different periods of *U. macrocarpa* populations occupied, we computed Schoener's *D* [78] and Hellinger distance *I* [79] using the ENMTOOLS [80]. The values of the two parameters varied from 0 (complete differentiation) to 1 (complete overlapping), which could be regarded as indicators for assessing the similarity of niches.

3. Results

3.1. Genetic Diversity and Differentiation

After alignment and manual correction, the concatenate chloroplast sequence was 1668 bp in length, including 41 polymorphic sites. A total of eighteen haplotypes were identified among 110 accessions (Figure 1; Table S1). The haplotypes H8 and H4 were the most widely distributed, shared by nine and eight populations, respectively, followed by H13 (shared by six populations). In contrast, the haplotypes H5, H6, H10, H12, H16, and H17 occurred in only single population. Most populations possessed multiple haplotypes, while only one haplotype (H8) was found in the SHHLC.

We observed the high genetic diversity of *U. macrocarpa* populations. The total haplotype diversity (*Hd*) and nucleotide diversity (π) were 0.901 and 0.0053, respectively. Furthermore, the genetic parameters h_T, h_S, V_T, and V_S were 0.889, 0.397, 0.893, and 0.292, respectively. For different populations, the haplotype diversity ranged from 0 to 0.9. The population YQS presented the highest nucleotide diversity, corresponding to 0.0072, followed by the population QS with the nucleotide diversity of 0.0063. However, the nucleotide diversity of the population SHHLC was 0, indicating that no genetic variation was detected within this population (Table S1).

The NJ tree (Figure 2a), PCA (Figure 2b), and STRUCTURE analysis (Figure 2c) consistently divided these populations into three groups. In the structure analysis, the ΔK had the highest value when $K = 3$, followed by $K = 2$ (Figure S1), indicating that the best grouping pattern was three among these populations. Moreover, the SAMOVA showed a higher F_{CT} value (0.5320) when $K = 3$ than that (0.48322) when $K = 2$, suggesting that the best geographical grouping was also three. As expected, we observed that three groups had a strong geographic basis (in group I, the population was mainly located in Shanxi, including KL, HCS, ZJS, WTS, QLY, HLMKZ, YQS, DGH, and MHS; in group II, the population mainly located in Hebei and Beijing, including DQG, DHS, HLS, QFS, XWTS, BHS, and SFS; in group III, the population was mainly located in Heilongjiang, Jilin, and Liaoning, including QS, SDLC, HXLC, MDF, JH, and SHHLC) (Figures 1 and 2; Table S1). The haplotype network presented a consistent geographic distribution pattern with the STRUCTURE and SAMOVA, in which the haplotypes originating from the same group had a closer relationship (Figure 1b). The genetic differentiation between populations was significantly higher when computed using a distance matrix than when using haplotype frequencies (N_{ST} (0.518) > G_{ST} (0.240), $p < 0.05$), indicating a significant phylogeographic structure within *U. macrocarpa*.
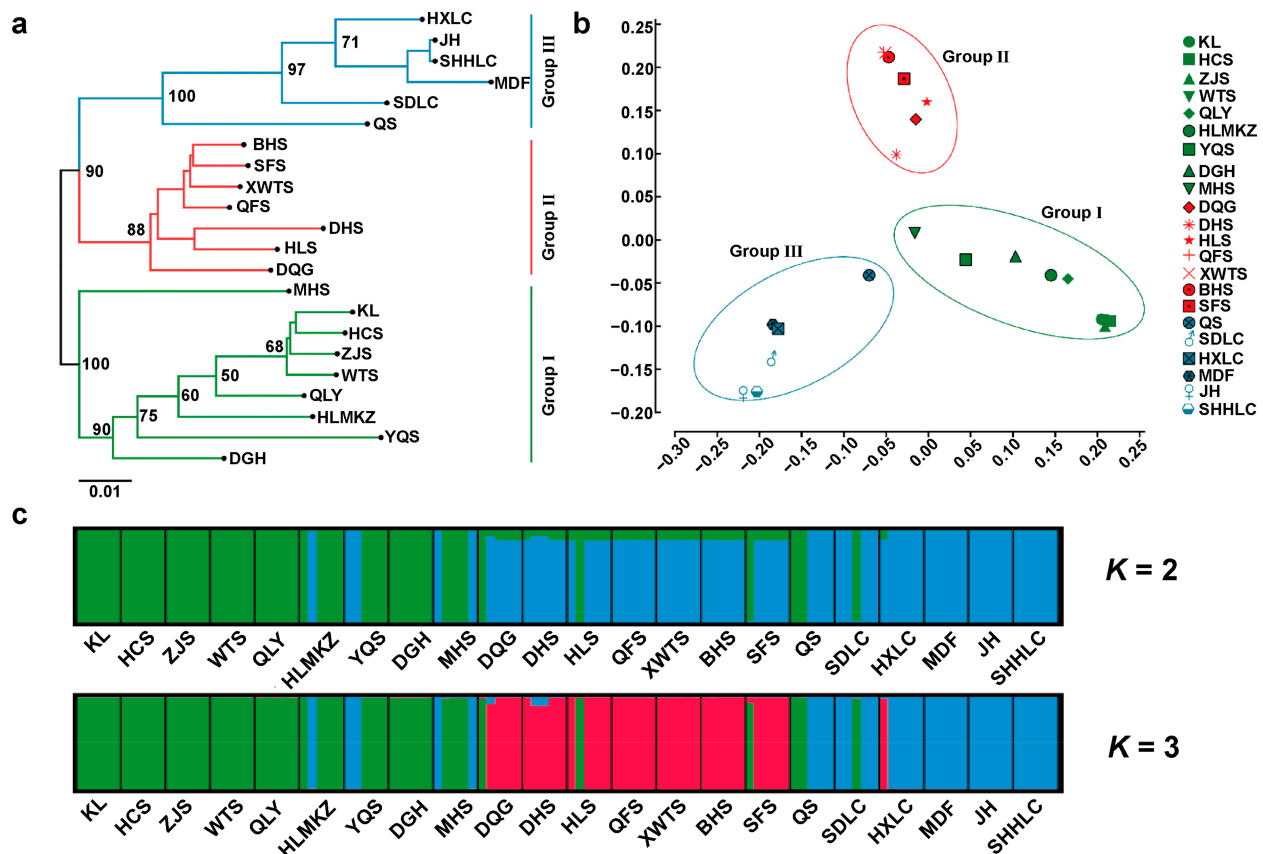
Figure 2. The genetic structure and phylogenic relationship of *U. macrocarpa* populations. (**a**) The population NJ tree of *U. macrocarpa*. (**b**) The PCA of *U. macrocarpa* populations. (**c**) The genetic structure for *K* = 2 and *K* = 3 for *U. macrocarpa* populations.

Furthermore, we investigated the genetic differentiation of these three *U. macrocarpa* phytogeographical groups in detail. The hierarchical AMOVA revealed that more than half the amount of variation (53%) occurred between three groups, and only 7% presented differences among populations within groups, whereas 40% of the variation was within populations (Table 1). The genetic differentiation between group I and group III was relatively high (F_{CT} = 0.587), followed by group II and group III (F_{CT} = 0.554) and group I and group II (F_{CT} = 0.440) (Table 1). We also found that the genetic differentiation among *U. macrocarpa* populations was significantly associated with geographical and climate isolation. Mantel tests and GLM (Figure 3) unveiled a significant correlation between genetic and geographic distance (r = 0.5137, R^2 = 0.2639, F = 82.08, *p* = 0.001) and between genetic and climatic distance (r = 0.1841, R^2 = 0.03389, F = 8.031, *p* = 0.005).

Table 1. Landscape of genetic variation within and among three identified groups.

	Source	df	SS	MS	Est. Var.	Var. Per. (%)	F-Statistic ($p < 0.05$)
Among three groups	Among Groups	2	86.067	43.034	1.147	53%	F_{CT} = 0.532
	Among Pops	19	30.051	1.582	0.143	7%	F_{SC} = 0.141
	Within Pops	88	76.400	0.868	0.868	40%	F_{ST} = 0.598
	Total	109	192.518		2.158	100%	
Group I vs. Group II	Among Groups	1	32.995	32.995	0.797	44%	F_{CT} = 0.440
	Among Pops	14	22.717	1.623	0.152	8%	F_{SC} = 0.150
	Within Pops	64	55.200	0.863	0.863	48%	F_{ST} = 0.524
	Total	79	110.913		1.811	100%	

Table 1. *Cont.*

	Source	df	SS	MS	Est. Var.	Var. Per. (%)	F-Statistic ($p < 0.05$)
Group I vs. Group III	Among Groups	1	60.684	60.684	1.634	59%	$F_{CT} = 0.587$ $F_{SC} = 0.155$ $F_{ST} = 0.651$
	Among Pops	13	24.222	1.863	0.178	6%	
	Within Pops	60	58.400	0.973	0.973	35%	
	Total	74	143.307		2.785	100%	
Group II vs. Group III	Among Groups	1	35.023	35.023	1.047	55%	$F_{CT} = 0.554$ $F_{SC} = 0.105$ $F_{ST} = 0.601$
	Among Pops	11	13.162	1.197	0.089	5%	
	Within Pops	52	39.200	0.754	0.754	40%	
	Total	64	87.385		1.889	100%	
Total	Among Pops	21	116.118	5.529	0.932	52%	$F_{ST} = 0.518$
	Within Pops	88	76.400	0.868	0.868	48%	
	Total	109	192.518		1.80	100%	

F_{CT}, genetic differentiation among groups; F_{SC}, genetic differentiation among populations within groups; F_{ST}, genetic differentiation among populations.

Figure 3. The distribution of pairwise F_{ST} along the geographic distance (**a**) and climatic distance (**b**), respectively. The red line represents the generalized linear model (GLM) equation (solid line) with 95% confidence interval (dotted line). (**a**) Genetic distance was positively correlated with geographic distance. GLM: Slope = 0.4269 (95% CI: 0.334–0.5198); Y-intercept = −0.7533 (95% CI: −1.015−−0.4917); X-intercept = 1.764 (95% CI: 1.465–1.961); R^2 = 0.2639; F = 82.08; p = 0.001. (**b**) Genetic distance was positively correlated with climatic distance. GLM: Slope = 0.3552 (95% CI: 0.1083–0.6022); Y-intercept = 0.3011 (95% CI: 0.1975–0.4048); X-intercept = −0.8477 (95% CI: −3.679−−0.3333); R^2 = 0.0339; F = 8.031; p = 0.005.

3.2. Phytogeographical Pattern and Demographic History

Demographic histories played an important role in shaping the current population's diversity pattern. The Bayesian Inference (BI) tree constructed by BEAST suggested that 18 putative haplotypes could also be divided into three groups (Figure 4), which was consistent with the haplotype network (Figure 1b) and population structure analysis (Figure 2). Group I consisted of ten haplotypes (H1, H2, H3, H4, H5, H6, H7, H9, H10, and H17), while groups II and III contained five (H12, H13, H14, H15, and H16) and three (H8, H11, and H18) haplotypes, respectively.
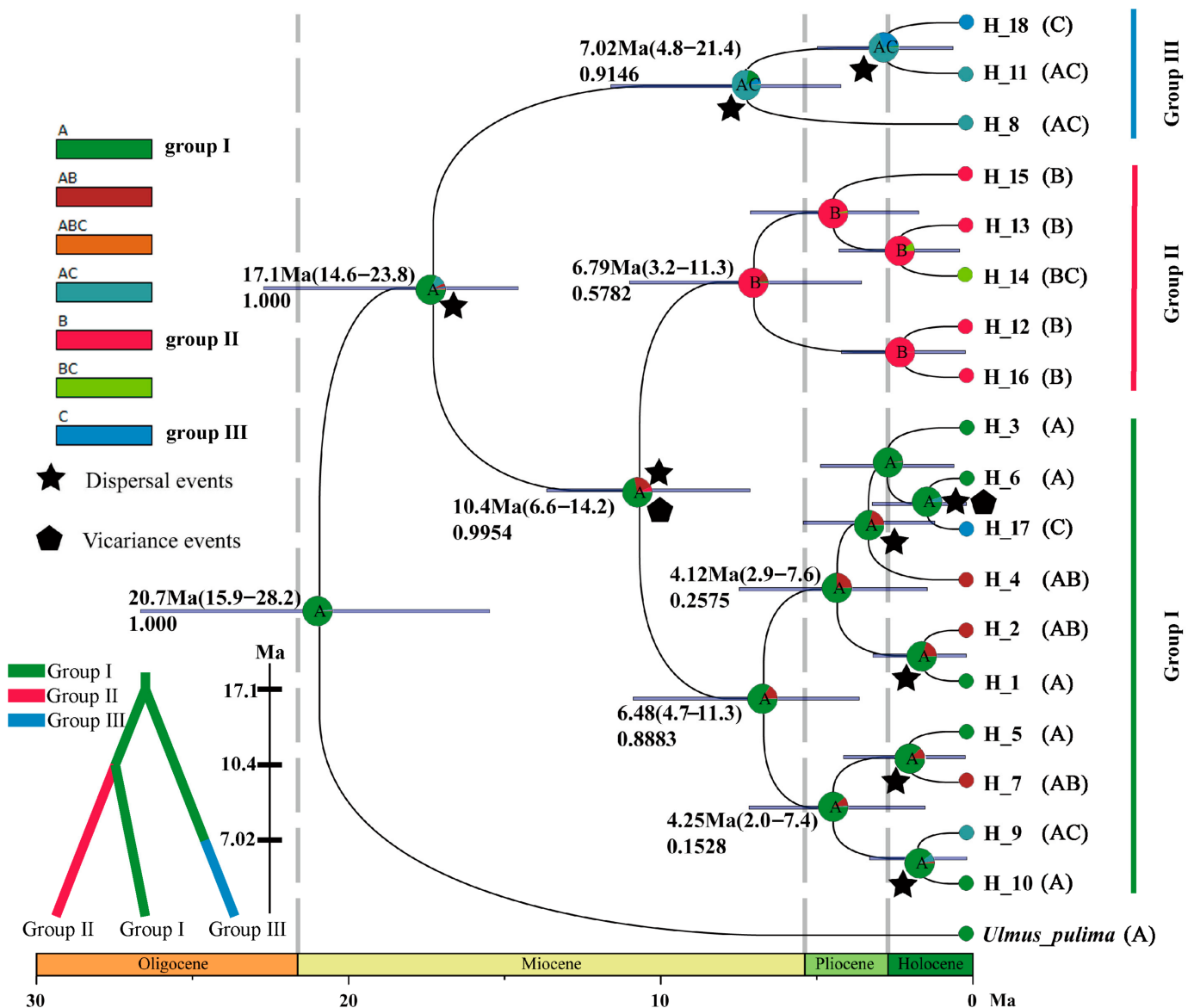
Figure 4. BEAST-derived phylogenetic relationships and ancestral distributions reconstruction by RASP analysis. On the BI tree, the numbers below nodes denoted a posterior probability, while the numbers above nodes indicated the divergence time with 95% highest posterior density (HPD).

The differentiation time of *U. macrocarpa* with the outgroup *U. pulima* was ~20.7 Ma (95% HPD: 15.9–28.2 Ma) in the middle Miocene. The divergence time of the most recent common ancestor of all *U. macrocarpa* haplotypes was estimated at ~17.1 Ma (95% HPD: 5.17–13.33 Ma). Subsequently, the divergence between group I and II occurred at ~10.4 Ma (95% HPD: 6.6–14.2 Ma). We observed that the diversification within each group all occurred in the late Miocene. Specifically, the divergence time within groups I, II, and III were estimated at 6.48 Ma, 6.79 Ma, and 7.02 Ma, respectively. Overall, the intragroup divergence continuously occurred from the later Miocene to Pliocene, where the approximate more recent differentiation time of the intragroup haplotypes for *U. macrocarpa* was during the Quaternary Era (e.g., H6 and H17, H12 and H16). According to the geographical distribution (Figure 1a) and genetic structure (Figures 1b and 2), all putative haplotypes were assigned to three states (labeled A–C) in RASP analysis (Figure 4). Akin to the results of divergence time estimation, state A was inferred as the relatively ancestral state of *U. macrocarpa*. Nine dispersal and four vicariance events were identified during the *U. macrocarpa* evolution. The common ancestral of *U. macrocarpa* experienced dispersal events

to form state C and the common ancestral of states A and B. Subsequently, vicariance and dispersal events were simultaneously defined as the splitting of an ancestral lineage into two descendant lineages (states A and B) that were divided between two adjacent regions.

Although the *U. macrocarpa* population, as well as the putative haplotypes, could be relatively divided into three phytogeographical groups (Figures 1, 2 and 4) with significant genetic differentiation (Table 1; Figure 3), we observed some stable admixtures among different groups (Figure 2c). Hence, we performed the MIGRATE and BAYESSAS analysis to explore the gene introgression between different groups (Table 2). The historical and contemporary gene flow ranged from 0.6250 to 1.3744 and 0.0068 to 0.0420, respectively. The historical and contemporary gene flows were relatively high between groups I and III.

Table 2. Rates of historical and contemporary gene flows per generation among three groups as calculated by the programs MIGRATE–N and BYESASS, respectively.

	Group I	Group II	Group III
		MIGRATE–N	
group I	-	0.6451 (0.4540–2.1406)	1.3744 (0.3632–2.9279)
group II	1.3054 (0.3393–2.7281)	-	0.6251 (0–2.0838)
group III	0.9069 (0.186–2.0686)	0.8154 (0.1240–2.0686)	-
		BAYESASS	
group I	0.9511 (0.9178–0.9844)	0.0342 (0.0015–0.9844)	0.0403 (0.0038–0.0768)
group II	0.0068 (0–0.0199)	0.9571 (0.9212–0.9930)	0.0201 (0–0.0464)
group III	0.0420 (0.0108–0.0732)	0.0086 (0–0.0256)	0.9396 (0.8971–0.9821)

Values in parentheses represent 95% confidence intervals.

3.3. Ecological Niche Modeling and Population Size Changing

Mismatch distributions analysis showed that the species experienced a recent expansion, as supported by uniformly non-significant SSD (0.0036, $p > 0.05$) and HRag (0.0154, $p > 0.05$) values, although Tajima's D (2.6327, $p > 0.05$) and Fu's FS (-2.7498, $p > 0.05$) values were not significant in neutrality test. To further explore the population dynamics of *U. macrocarpa*, ecological niche modeling was performed using the MAXENT method.

After filtering, six reserved climate variables (bio2, bio7, bio8, bio12, bio14, and bio15) had a dominant influence (percentage contribution = 87.6%) on the geographic distribution of *U. macrocarpa*. Furthermore, the high AUC values (>0.900) indicated that all MAXENT models exhibited high predictive ability.

The predictions of the current distribution for *U. macrocarpa* fit relatively well with its actual distribution (Figure 5) in Northern China, including Shaanxi, Shanxi, Shandong, Hebei, and Liaoning. During the LGM, the potential distribution of *U. macrocarpa* was smaller than that at present. The relatively lower D (0.7229) and I (0.9306) values indicated a significant niche differentiation between the LGM and the current period (Table 3). During the LIG, the potential range of this species was more extensive than that of the current period, with a northern expansion. The *U. macrocarpa* occupied more suitable northerly habitat areas such as Inner Mongolia in this period.

Table 3. Degree of niche overlap based on Schoener's *D* and Hellinger distance *I* statistics.

	Current	MH	LGM	LIG
Current	-	0.9647 [+]	0.9500 [+]	0.9306 [+]
MH	0.8155 [*]	-	0.9563 [+]	0.9265 [+]
LGM	0.7900 [*]	0.7924 [*]	-	0.9327 [+]
LIG	0.7218 [*]	0.7229 [*]	0.7341 [*]	-

The "*" represent the *D* value, and the "+" represent the *I* value.
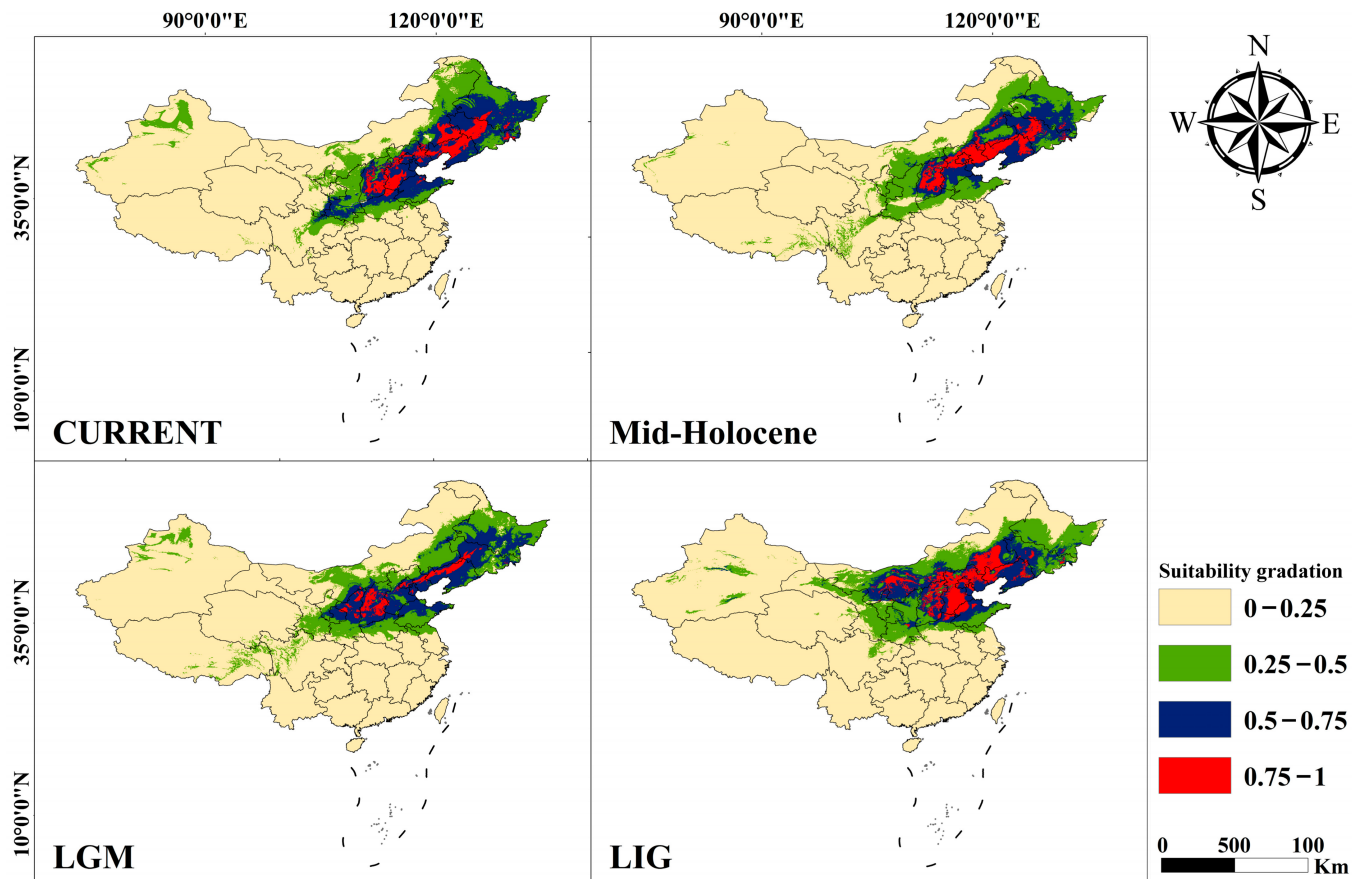
Figure 5. The estimated geographic distribution of *U. macrocarpa* in the current, Mid-Holocene, LGM, and LIG. Different colors correspond to different grades of suitability.

4. Discussion

4.1. High Genetic Diversity and Significant Genetic Differentiation of U. macrocarpa

Genetic diversity serves as the foundational material essential for biological evolution and represents the predominant origin of biodiversity [81]. High genetic diversity for species represents a successful adaptive strategy for coping with diverse habitats and environmental conditions, thereby enhancing the ability of plants or populations to access and establish in novel habitats [82]. In this study, high levels of genetic diversity were observed in *U. macrocarpa* populations (Table S1), consistent with the rich phenotypic diversity of this species in previous studies [24]. The total gene diversity of *U. macrocarpa* ($h_T = 0.889$) was higher than the mean total gene diversity ($h_T = 0.67$) detected in 170 plant species, of which chloroplast DNA markers have been used [83]. The observed high genetic diversity of *U. macrocarpa* populations is likely attributable to the gradual accumulation of nucleotide mutations over extended evolutionary periods. Generally, widespread species tend to exhibit greater genetic variability compared to those with limited distributions. [84]. As a dominant tree species in forest communities, *U. macrocarpa* is widely distributed across Northern China, leading to high genetic diversity.

A significant phylogeographic structure (N_{ST} (0.518) > G_{ST} (0.240), $p < 0.05$) was found in *U. macrocarpa*. Subsequently, the clustering analysis (Figure 2) and SMOVA consistently divided *U. macrocarpa* populations into three groups with significant genetic differentiation (Table 1). Numerous factors influence the genetic differentiation among plant populations, with geographical isolation and climatic heterogeneity identified as pivotal drivers [84]. Spatial heterogeneity of the environment exerts differential selection pressures on natural populations, potentially leading to the rapid differentiation of populations [85,86]. Our study found significant Isolation-by-Distance and Isolation-by-Environment patterns via

the Mantel test (Figure 3). The topography in Northern China is highly diversified. The uplifts of mountains such as Taihang, Yanshan, and Yinshan in Northern China have served as practical barriers to prevent dispersal and introgression, thus promoting genetic diversification of species. With geographical isolation, the split *U. macrocarpa* populations gradually adapted to local climate conditions. Additionally, *U. macrocarpa* is dioecious and wind-pollinated, limiting pollen dispersal to short distances. Consequently, the diminished gene flow (Table 2) due to habitat fragmentation has resulted in pronounced genetic divergence among *U. macrocarpa* populations in Northern China.

4.2. Demographic History Inference of U. macrocarpa

The populations of *U. macrocarpa* had a significant phylogeographic pattern (Figures 1 and 2). The mismatch distributions analysis of the chloroplast sequence indicated that the *U. macrocarpa* populations experienced a recent expansion (SSD = 0.0036, $p > 0.05$; HRag = 0.0154, $p > 0.05$), which was consistent with the repaid diversification of *U. macrocarpa* during late Miocene to Quaternary (Figure 4). However, in previous studies, researchers suggested that the *U. macrocarpa*'s close relatives, *U. lamellosa,* did not undergo a significant expansion due to the limitation of uplift of mountains and complex geological conditions in Northern China [10,36]. We speculated that the high ecological adaptability of *U. macrocarpa* was the primary reason for its expansion to a broad range and the occupying of multiple gradient niches (Figures 1 and 5) [24,25]. Additionally, the absence of a continuous ice sheet in Northern China in the Quaternary allowed for population expansion during the post-glacial recolonization and dispersal (Figure 5).

Based on the fossil calibration, although the intraspecific divergence of all *U. macrocarpa* haplotypes (17.1 Ma, 95% HPD: 14.6–23.8 Ma) most probably began during the early stage of middle Miocene (Figure 4), the blooming diversification within three *U. macrocarpa* phytogeographic groups occurred mainly during the late Miocene to Pliocene. This period is an important differentiation epoch for tree species in China. Evidence supporting late Miocene and Pliocene diversification of other temperate tree species has also been documented in many phytogeographic studies, such as *Acer* [87], *Cercidiphyllum* [88], and *Juglans* [2,89]. The uplift of the Tibetan–Himalayan Plateau in the late Miocene is seen as a key factor in triggering the diversification of plants in China due to changes in the Asian monsoon circulation, aridification in Central Asia, and China's complex topography (~10–7 Ma) [90–92]. Northern China was impacted by both global climate change and the spread of aridity from West to East [93]. We speculated that the diversification of *U. macrocarpa* haplotypes was associated with the monsoon circulation and aridification in Northern China during this period.

Additionally, the deformation of mountains located in Northern China, such as the Taihang, Yanshan, Yinshan, and Changbai Mountains, simultaneously occurred with the significant uplift of the Tibetan–Himalayan Plateau [94,95]. In addition to severing as geographical barriers, these mountains sometimes provided dispersal corridors, allowing for range expansions and population connectivity [96,97]. For example, during the Miocene, the uplift height of the northern part of the Taihang Mountains was merely half that of the western zone of the Yanshan Mountains [98]. The relatively modest elevation of the Taihang Mountains did not pose as a geographical barrier, thus failing to obstruct the migration of *U. macrocarpa*, which was consistent with the results of the RASP analysis (Figure 4). The *U. macrocarpa* ancestral group I, mainly distributed in Shanxi and Henan provinces (Table S1; Figure 1), crossed the Taihang Mountains corridor and spread to Hebei and further northeast regions such as Heilongjiang and Jilin provinces, leading to the global diversification landscape of *U. macrocarpa* in Northern China.

4.3. Potential Refugia under the Climate Oscillation in Quaternary

The Quaternary glacial–interglacial cycles had significant impacts on the differentiation and migration patterns of species [99]. The onset of certain haplotype divergence was more recent (Figure 4), implying that historical processes and climatic oscillations during

the Quaternary period have also shaped the present-day distribution of *U. macrocarpa*. Akin to other temperate tree species, Quaternary climatic oscillations and associated environmental changes may have made the diversification within *U. macrocarpa* in Northern China relatively complicated [2,10,36,84,89], which was also supported by the ecological niche modeling (Figure 5).

The climatic oscillations resulting from multiple glaciations have led to shifts in the distribution of *U. macrocarpa* and the isolation of populations, potentially resulting in the development of distinct population structures characterized as "southern richness" and "northern purity" [10]. As expected, during the LGM, the *U. macrocarpa* distribution, showing a southward trend, was significantly smaller than those of the present day, as well as the LIG (Table 3; Figure 5), which was consistent with the previous study [36]. Furthermore, multiple geographically isolated refugia existed for forests across East Asia in LGM, which promoted intraspecific divergence and led to their speciation and diversification [14,99]. Under the glaciations, refugia are ideal habitats for conserving genetic diversity and generating unique alleles. Therefore, geographic areas displaying increased levels of genetic diversity are, thus, good candidates in the search for past refugia [100].

In this study, we speculated that the surrounding areas of Shanxi and Inner Mongolia, where the group I mainly located, might be the major glacial refugia for *U. macrocarpa*. In addition to being the relatively ancestral group (Figure 4), it also possessed a higher haplotype and genetic diversity (Hd = 0.8666, π = 0.00368) than that of groups II (Hd = 0.7176, π = 0.00210) and III (Hd = 0.58391, π = 0.00295). The ecological niche modeling showed a highly suitable level, especially in Shanxi, for *U. macrocarpa* during the LGM (Figure 5). Interestingly, we found that haplotype 4 was the most dominant in group I (Figure 1; Table S1), occurring in eight populations (seven in Shanxi and one in Inner Mongolia) and located at the center of group I in the haplotype network. Furthermore, the populations with haplotype 4, such as YQS and HLMKZ, had higher haplotype and genetic diversity (Table S1). These results further indicated the reliability of refugia.

We also observed that haplotypes 13 and 8 were widely distributed in groups II and III, respectively (Figure 1; Table S1). Each phylogeographical group contained its unique dominant haplotype with high differentiation from each other (Figures 1 and 2; Table 1 and Table S1), indicating a parallel evolution pattern of *U. macrocarpa* populations in Northern China. The Taihang and Yanshan Mountains were uplifted sharply along with the Himalayan orogeny movement to finally form in the Quaternary [84], which dramatically resisted the recent gene flow between different groups (Table 2), thus leading to the parallel evolution pattern within each group of *U. macrocarpa*.

5. Conclusions

In this study, using chloroplast DNA, we analyzed the phytogeography and demographical history of the temperate tree species *U. macrocarpa*. The results showed that *U. macrocarpa* had a significant phylogeographical structure with high genetic diversity. A total of 18 putative haplotypes were divided into three groups. The divergence of intraspecies haplotypes occurred during the Miocene–Pliocene, which was associated with major Tertiary geological and/or climatic events in Northern China. Quaternary climatic oscillations also significantly impacted the distribution of *U. macrocarpa*. The surrounding areas of Shanxi and Inner Mongolia might be regarded as refugia for *U. macrocarpa* in the glacial period. The uplift of mountains in the Quaternary resisted the gene flow between different phylogeographical groups, leading to a potential parallel evolution pattern of *U. macrocarpa* populations in Northern China. Our results broaden our understanding of the demographical history and genetic architecture of forests in Northern China.

References

1. Hewitt, G. The genetic legacy of the Quaternary ice ages. *Nature* **2000**, *405*, 907–913. [CrossRef] [PubMed]
2. Bai, W.-N.; Wang, W.-T.; Zhang, D.-Y. Phylogeographic breaks within Asian butternuts indicate the existence of a phytogeographic divide in East Asia. *New Phytol.* **2016**, *209*, 1757–1772. [CrossRef] [PubMed]
3. Bai, W.-N.; Liao, W.-J.; Zhang, D.-Y. Nuclear and chloroplast DNA phylogeography reveal two refuge areas with asymmetrical gene flow in a temperate walnut tree from East Asia. *New Phytol.* **2010**, *188*, 892–901. [CrossRef]
4. Feng, L.; Du, F.K. Landscape Genomics in Tree Conservation Under a Changing Environment. *Front. Plant Sci.* **2022**, *13*, 822217. [CrossRef] [PubMed]
5. Pennington, P.T.; Cronk, Q.C.B.; Richardson, J.A.; Donoghue, M.J.; Smith, S.A. Patterns in the assembly of temperate forests around the Northern Hemisphere. Philosophical Transactions of the Royal Society of London. *Ser. B Biol. Sci.* **2004**, *359*, 1633–1644. [CrossRef] [PubMed]
6. Xiang, J.-Y.; Wen, J.; Peng, H. Evolution of the eastern Asian–North American biogeographic disjunctions in ferns and lycophytes. *J. Syst. Evol.* **2015**, *53*, 2–32. [CrossRef]
7. Wolfe, J.A. Tertiary climates and floristic relationships at high latitudes in the northern hemisphere. *Palaeogeogr. Palaeoclimatol. Palaeoecol.* **1980**, *30*, 313–323. [CrossRef]
8. Husemann, M.; Guzman, N.V.; Danley, P.D.; Cigliano, M.M.; Confalonieri, V.A. Biogeography of *Trimerotropis pallidipennis* (Acrididae: Oedipodinae): Deep divergence across the Americas. *J. Biogeogr.* **2013**, *40*, 261–273. [CrossRef]
9. Wang, J.; Källman, T.; Liu, J.; Guo, Q.; Wu, Y.; Lin, K.; Lascoux, M. Speciation of two desert poplar species triggered by Pleistocene climatic oscillations. *Heredity* **2014**, *112*, 156–164. [CrossRef] [PubMed]
10. Hou, H.; Ye, H.; Wang, Z.; Wu, J.; Gao, Y.; Han, W.; Na, D.; Sun, G.; Wang, Y. Demographic history and genetic differentiation of an endemic and endangered *Ulmus lamellosa* (Ulmus). *BMC Plant Biol.* **2020**, *20*, 526. [CrossRef]
11. Qiu, Y.-X.; Fu, C.-X.; Comes, H.P. Plant molecular phylogeography in China and adjacent regions: Tracing the genetic imprints of Quaternary climate and environmental change in the world's most diverse temperate flora. *Mol. Phylogenetics Evol.* **2011**, *59*, 225–244. [CrossRef] [PubMed]
12. Zeng, Y.-F.; Zhang, J.-G.; Abuduhamiti, B.; Wang, W.-T.; Jia, Z.-Q. Phylogeographic patterns of the desert poplar in Northwest China shaped by both geology and climatic oscillations. *BMC Evol. Biol.* **2018**, *18*, 75. [CrossRef] [PubMed]
13. Stewart, J.R.; Lister, A.M.; Barnes, I.; Dalén, L. Refugia revisited: Individualistic responses of species in space and time. *Proc. R. Soc. B Biol. Sci.* **2010**, *277*, 661–671. [CrossRef] [PubMed]
14. Chen, T.-Y.; Lou, A.-R. Phylogeography and paleodistribution models of a widespread birch (*Betula platyphylla* Suk.) across East Asia: Multiple refugia, multidirectional expansion, and heterogeneous genetic pattern. *Ecol. Evol.* **2019**, *9*, 7792–7807. [CrossRef] [PubMed]
15. Tian, B.; Liu, R.; Wang, L.; Qiu, Q.; Chen, K.; Liu, J. Phylogeographic analyses suggest that a deciduous species (*Ostryopsis davidiana* Decne., Betulaceae) survived in northern China during the Last Glacial Maximum. *J. Biogeogr.* **2009**, *36*, 2148–2155. [CrossRef]
16. Liu, H.-Z.; Harada, K. Geographic distribution and origin of the chloroplast T/C-type in *Quercus mongolica* var. crispula in northeastern Japan. *Plant Species Biol.* **2014**, *29*, 207–211. [CrossRef]

17. Zhang, Y.-H.; Wang, I.J.; Comes, H.P.; Peng, H.; Qiu, Y.-X. Contributions of historical and contemporary geographic and environmental factors to phylogeographic structure in a Tertiary relict species, *Emmenopterys henryi* (Rubiaceae). *Sci. Rep.* **2016**, *6*, 24041. [CrossRef]

18. Favre, A.; Päckert, M.; Pauls, S.U.; Jähnig, S.C.; Uhl, D.; Michalak, I.; Muellner-Riehl, A.N. The role of the uplift of the Qinghai-Tibetan Plateau for the evolution of Tibetan biotas. *Biol. Rev.* **2015**, *90*, 236–253. [CrossRef] [PubMed]

19. Xing, Y.; Gandolfo, M.A.; Onstein, R.E.; Cantrill, D.J.; Jacobs, B.F.; Jordan, G.J.; Lee, D.E.; Popova, S.; Srivastava, R.; Su, T.; et al. Testing the Biases in the Rich Cenozoic Angiosperm Macrofossil Record. *Int. J. Plant Sci.* **2016**, *177*, 371–388. [CrossRef]

20. Fragnière, Y.; Song, Y.-G.; Fazan, L.; Manchester, S.R.; Garfi, G.; Kozlowski, G. Biogeographic Overview of Ulmaceae: Diversity, Distribution, Ecological Preferences, and Conservation Status. *Plants* **2021**, *10*, 1111. [CrossRef] [PubMed]

21. Zhang, Q.-Y.; Deng, M.; Bouchenak-Khelladi, Y.; Zhou, Z.-K.; Hu, G.-W.; Xing, Y.-W. The diversification of the northern temperate woody flora—A case study of the Elm family (Ulmaceae) based on phylogenomic and paleobotanical evidence. *J. Syst. Evol.* **2022**, *60*, 728–746. [CrossRef]

22. Wang, S.; Zuo, L.; Liu, Y.; Long, L.; Wu, J.; Yuan, M.; Wang, J.; Yang, M. Comparative transcriptomes of four Elm species provide insights into the genetic features and adaptive evolution of *Ulmus* spp. *For. Ecol. Manag.* **2024**, *553*, 121560. [CrossRef]

23. Fu, L.; Chen, J.; Tang, Y. Materiae ad floram Ulmacearum Sinensium. *Acta Phytotaxon. Sin.* **1979**, *17*, 45–51.

24. Yan, D. Leaf Morphological Differences of *Ulmus macrocarpa*. Master's Thesis, Shanxi Normal University, Taiyuan, China, 2018.

25. Fu, L. Research on the *Ulmus* genus in China. *J. Northeast For. Univ.* **1980**, *3*, 1–40.

26. Lee, I.; Kwon, D.H.; Lee, S.H.; Lee, S.D.; Kim, D.W.; Lee, J.-H.; Hyun, S.K.; Kang, K.H.; Kim, C.; Kim, B.W.; et al. Immune-modulation Effect of *Ulmus macrocarpa* Hance Water Extract on Balb/c Mice. *J. Life Sci.* **2014**, *24*, 1151–1156. [CrossRef]

27. Han, H.-J.; Song, X.; Yadav, D.; Hwang, M.S.; Lee, J.H.; Lee, C.H.; Kim, T.H.; Lee, J.J.; Kwon, J. *Ulmus macrocarpa* Hance modulates lipid metabolism in hyperlipidemia via activation of AMPK pathway. *PLoS ONE* **2019**, *14*, e0217112. [CrossRef] [PubMed]

28. Brunet, J.; Zalapa, J.; Guries, R. Conservation of genetic diversity in slippery elm (*Ulmus rubra*) in Wisconsin despite the devastating impact of Dutch elm disease. *Conserv. Genet.* **2016**, *17*, 1001–1010. [CrossRef]

29. Zalapa, J.E.; Brunet, J.; Guries, R.P. Genetic diversity and relationships among Dutch elm disease tolerant *Ulmus pumila* L. accessions from China. *Genome* **2008**, *51*, 492–500. [CrossRef]

30. Machon, N.; Lefranc, M.; Bilger, I.; Mazer, S.J.; Sarr, A. Allozyme variation in *Ulmus* species from France: Analysis of differentiation. *Heredity* **1997**, *78*, 12–20. [CrossRef] [PubMed]

31. Martín del Puerto, M.; Martínez García, F.; Mohanty, A.; Martín, J.P. Genetic Diversity in Relict and Fragmented Populations of *Ulmus glabra* Hudson in the Central System of the Iberian Peninsula. *Forests* **2017**, *8*, 143. [CrossRef]

32. Khan, R.U.; Ali, N.; Rahman, S.U.; Rahman, I.U.; Hashem, A.; Almutairi, K.F.; Fathi Abd_Allah, E.; Harsonowati, W.; Khan, M.A.; Rahim, F.; et al. Genetic Diversity and Population Structure of the Endangered Ulmusvillosa in Pakistan Revealed by DNA Barcode Markers. *Appl. Sci.* **2022**, *12*, 9293. [CrossRef]

33. Chen, P.; Liu, P.; Zhang, Q.; Bu, C.; Lu, C.; Srivastava, S.; Zhang, D.; Song, Y. Gene Coexpression Network Analysis Indicates that Hub Genes Related to Photosynthesis and Starch Synthesis Modulate Salt Stress Tolerance in *Ulmus pumila*. *Int. J. Mol. Sci.* **2021**, *22*, 4410. [CrossRef] [PubMed]

34. Islam, M.T.; Coutin, J.F.; Shukla, M.; Dhaliwal, A.K.; Nigg, M.; Bernier, L.; Sherif, S.M.; Saxena, P.K. Deciphering the Genome-Wide Transcriptomic Changes during Interactions of Resistant and Susceptible Genotypes of American Elm with *Ophiostoma novo-ulmi*. *J. Fungi* **2022**, *8*, 120. [CrossRef]

35. Zhang, L.; Xie, S.; Yang, C.; Cao, D.; Fan, S.; Zhang, X. Comparative Transcriptome Analysis Reveals Candidate Genes and Pathways for Potential Branch Growth in Elm (*Ulmus pumila*) Cultivars. *Biology* **2022**, *11*, 711. [CrossRef] [PubMed]

36. Liu, L.; Chen, W.; Yan, D.-T.; Li, J.; Liu, L.; Wang, Y.-L. Molecular phylogeography and paleodistribution modeling of the boreal tree species *Ulmus lamellosa* (T. Wang et S. L. Chang) (Ulmaceae) in China. *Tree Genet. Genomes* **2017**, *13*, 11. [CrossRef]

37. Dong, W.; Xu, C.; Li, C.; Sun, J.; Zuo, Y.; Shi, S.; Cheng, T.; Guo, J.; Zhou, S. ycf1, the most promising plastid DNA barcode of land plants. *Sci. Rep.* **2015**, *5*, 8348. [CrossRef] [PubMed]

38. Drescher, A.; Ruf, S.; Calsa, T., Jr.; Carrer, H.; Bock, R. The two largest chloroplast genome-encoded open reading frames of higher plants are essential genes. *Plant J.* **2000**, *22*, 97–104. [CrossRef] [PubMed]

39. Jiang, D.; Cai, X.; Gong, M.; Xia, M.; Xing, H.; Dong, S.; Tian, S.; Li, J.; Lin, J.; Liu, Y.; et al. Complete chloroplast genomes provide insights into evolution and phylogeny of *Zingiber* (Zingiberaceae). *BMC Genom.* **2023**, *24*, 30. [CrossRef] [PubMed]

40. Kim, G.-B.; Lim, C.E.; Kim, J.-S.; Kim, K.; Lee, J.H.; Yu, H.-J.; Mun, J.-H. Comparative chloroplast genome analysis of *Artemisia* (Asteraceae) in East Asia: Insights into evolutionary divergence and phylogenomic implications. *BMC Genom.* **2020**, *21*, 415. [CrossRef] [PubMed]

41. Amar, M.H. ycf1-ndhF genes, the most promising plastid genomic barcode, sheds light on phylogeny at low taxonomic levels in *Prunus persica*. *J. Genet. Eng. Biotechnol.* **2020**, *18*, 42. [CrossRef] [PubMed]

42. Li, H.; Xiao, W.; Tong, T.; Li, Y.; Zhang, M.; Lin, X.; Zou, X.; Wu, Q.; Guo, X. The specific DNA barcodes based on chloroplast genes for species identification of Orchidaceae plants. *Sci. Rep.* **2021**, *11*, 1424. [CrossRef] [PubMed]

43. Dong, W.; Liu, J.; Yu, J.; Wang, L.; Zhou, S. Highly Variable Chloroplast Markers for Evaluating Plant Phylogeny at Low Taxonomic Levels and for DNA Barcoding. *PLoS ONE* **2012**, *7*, e35071. [CrossRef] [PubMed]

44. Neubig, K.M.; Whitten, W.M.; Carlsward, B.S.; Blanco, M.A.; Endara, L.; Williams, N.H.; Moore, M. Phylogenetic utility of *ycf1* in orchids: A plastid gene more variable than *matK*. *Plant Syst. Evol.* **2009**, *277*, 75–84. [CrossRef]

45. Shaw, J.; Lickey, E.B.; Schilling, E.E.; Small, R.L. Comparison of whole chloroplast genome sequences to choose noncoding regions for phylogenetic studies in angiosperms: The tortoise and the hare III. *Am. J. Bot.* **2007**, *94*, 275–288. [CrossRef]

46. Chiang, T.-Y.; Schaal, B.A. Molecular evolution and phylogeny of the atpB-rbcL spacer of chloroplast DNA in the true mosses. *Genome* **2000**, *43*, 417–426. [CrossRef] [PubMed]

47. Demesure, B.; Sodzi, N.; Petit, R.J. A set of universal primers for amplification of polymorphic non-coding regions of mitochondrial and chloroplast DNA in plants. *Mol. Ecol.* **1995**, *4*, 129–134. [CrossRef]

48. Allen, G.C.; Flores-Vergara, M.A.; Krasynanski, S.; Kumar, S.; Thompson, W.F. A modified protocol for rapid DNA isolation from plant tissues using cetyltrimethylammonium bromide. *Nat. Protoc.* **2006**, *1*, 2320–2325. [CrossRef]

49. Singh, V.K.; Mangalam, A.K.; Dwivedi, S.; Naik, S. Primer Premier: Program for Design of Degenerate Primers from a Protein Sequence. *BioTechniques* **1998**, *24*, 318–319. [CrossRef] [PubMed]

50. Katoh, K.; Misawa, K.; Kuma, K.-i.; Miyata, T. MAFFT: A novel method for rapid multiple sequence alignment based on fast Fourier transform. *Nucleic Acids Res.* **2002**, *30*, 3059–3066. [CrossRef] [PubMed]

51. Castresana, J. Selection of Conserved Blocks from Multiple Alignments for Their Use in Phylogenetic Analysis. *Mol. Biol. Evol.* **2000**, *17*, 540–552. [CrossRef]

52. Rozas, J.; Sánchez-DelBarrio, J.C.; Messeguer, X.; Rozas, R. DnaSP, DNA polymorphism analyses by the coalescent and other methods. *Bioinformatics* **2003**, *19*, 2496–2497. [CrossRef] [PubMed]

53. Pons, O.; Petit, R.J. Measuring and testing genetic differentiation with ordered versus unordered alleles. *Genetics* **1996**, *144*, 1237–1245. [CrossRef] [PubMed]

54. Excoffier, L.; Lischer, H.E.L. Arlequin suite ver 3.5: A new series of programs to perform population genetics analyses under Linux and Windows. *Mol. Ecol. Resour.* **2010**, *10*, 564–567. [CrossRef]

55. Takezaki, N.; Nei, M.; Tamura, K. POPTREE2: Software for Constructing Population Trees from Allele Frequency Data and Computing Other Population Statistics with Windows Interface. *Mol. Biol. Evol.* **2009**, *27*, 747–752. [CrossRef] [PubMed]

56. Peakall, R.; Smouse, P.E. GenAlEx 6.5: Genetic analysis in Excel. Population genetic software for teaching and research—An update. *Bioinformatics* **2012**, *28*, 2537–2539. [CrossRef] [PubMed]

57. Pritchard, J.K.; Stephens, M.; Donnelly, P. Inference of Population Structure Using Multilocus Genotype Data. *Genetics* **2000**, *155*, 945–959. [CrossRef] [PubMed]

58. Earl, D.A.; vonHoldt, B.M. STRUCTURE HARVESTER: A website and program for visualizing STRUCTURE output and implementing the Evanno method. *Conserv. Genet. Resour.* **2012**, *4*, 359–361. [CrossRef]

59. Jakobsson, M.; Rosenberg, N.A. CLUMPP: A cluster matching and permutation program for dealing with label switching and multimodality in analysis of population structure. *Bioinformatics* **2007**, *23*, 1801–1806. [CrossRef] [PubMed]

60. Rosenberg, N.A. DISTRUCT: A program for the graphical display of population structure. *Mol. Ecol. Notes* **2004**, *4*, 137–138. [CrossRef]

61. Dupanloup, I.; Schneider, S.; Excoffier, L. A simulated annealing approach to define the genetic structure of populations. *Mol. Ecol.* **2002**, *11*, 2571–2581. [CrossRef] [PubMed]

62. Leigh, J.W.; Bryant, D. POPART: Full-feature software for haplotype network construction. *Methods Ecol. Evol.* **2015**, *6*, 1110–1116. [CrossRef]

63. Dixon, P. VEGAN, a package of R functions for community ecology. *J. Veg. Sci.* **2003**, *14*, 927–930. [CrossRef]

64. Rosenberg, M.S.; Anderson, C.D. PASSaGE: Pattern Analysis, Spatial Statistics and Geographic Exegesis. Version 2. *Methods Ecol. Evol.* **2011**, *2*, 229–232. [CrossRef]

65. Drummond, A.J.; Suchard, M.A.; Xie, D.; Rambaut, A. Bayesian Phylogenetics with BEAUti and the BEAST 1.7. *Mol. Biol. Evol.* **2012**, *29*, 1969–1973. [CrossRef] [PubMed]

66. Darriba, D.; Taboada, G.L.; Doallo, R.; Posada, D. jModelTest 2: More models, new heuristics and parallel computing. *Nat. Methods* **2012**, *9*, 772. [CrossRef] [PubMed]

67. Posada, D.; Buckley, T.R. Model Selection and Model Averaging in Phylogenetics: Advantages of Akaike Information Criterion and Bayesian Approaches Over Likelihood Ratio Tests. *Syst. Biol.* **2004**, *53*, 793–808. [CrossRef] [PubMed]

68. Wolfe, K.H.; Li, W.H.; Sharp, P.M. Rates of nucleotide substitution vary greatly among plant mitochondrial, chloroplast, and nuclear DNAs. *Proc. Natl. Acad. Sci. USA* **1987**, *84*, 9054–9058. [CrossRef] [PubMed]

69. Liu, Y.; Guo, S.; Ferguson, D.K. Catalogue of Cenozoic megafossil plants in China. *Palaeontogr. Abt. B* **1996**, *238*, 141–179.

70. Tajima, F. Statistical method for testing the neutral mutation hypothesis by DNA polymorphism. *Genetics* **1989**, *123*, 585–595. [CrossRef]

71. Fu, Y.-X. Statistical Tests of Neutrality of Mutations Against Population Growth, Hitchhiking and Background Selection. *Genetics* **1997**, *147*, 915–925. [CrossRef] [PubMed]

72. Yu, Y.; Blair, C.; He, X. RASP 4: Ancestral State Reconstruction Tool for Multiple Genes and Characters. *Mol. Biol. Evol.* **2019**, *37*, 604–606. [CrossRef] [PubMed]

73. Beerli, P. Comparison of Bayesian and maximum-likelihood inference of population genetic parameters. *Bioinformatics* **2005**, *22*, 341–345. [CrossRef] [PubMed]

74. Wilson, G.A.; Rannala, B. Bayesian Inference of Recent Migration Rates Using Multilocus Genotypes. *Genetics* **2003**, *163*, 1177–1191. [CrossRef] [PubMed]

75. Phillips, S.J.; Dudík, M. Modeling of species distributions with Maxent: New extensions and a comprehensive evaluation. *Ecography* **2008**, *31*, 161–175. [CrossRef]

76. Naimi, B.; Hamm, N.A.S.; Groen, T.A.; Skidmore, A.K.; Toxopeus, A.G. Where is positional uncertainty a problem for species distribution modelling? *Ecography* **2014**, *37*, 191–203. [CrossRef]

77. Cornille, A.; Giraud, T.; Bellard, C.; Tellier, A.; Le Cam, B.; Smulders, M.J.M.; Kleinschmit, J.; Roldan-Ruiz, I.; Gladieux, P. Postglacial recolonization history of the European crabapple (*Malus sylvestris* Mill.), a wild contributor to the domesticated apple. *Mol. Ecol.* **2013**, *22*, 2249–2263. [CrossRef] [PubMed]

78. Schoener, T.W. The Anolis Lizards of Bimini: Resource Partitioning in a Complex Fauna. *Ecology* **1968**, *49*, 704–726. [CrossRef]

79. Warren, D.L.; Glor, R.E.; Turelli, M. Environmental niche equivalency versus conservatism: Quantitative approaches to niche evolution. *Evolution* **2008**, *62*, 2868–2883. [CrossRef] [PubMed]

80. Warren, D.L.; Glor, R.E.; Turelli, M. ENMTools: A toolbox for comparative studies of environmental niche models. *Ecography* **2010**, *33*, 607–611. [CrossRef]

81. Hughes, A.R.; Inouye, B.D.; Johnson, M.T.; Underwood, N.; Vellend, M. Ecological consequences of genetic diversity. *Ecol. Lett.* **2008**, *11*, 609–623. [CrossRef] [PubMed]

82. Deli, T.; Kiel, C.; Schubart, C.D. Phylogeographic and evolutionary history analyses of the warty crab *Eriphia verrucosa* (Decapoda, Brachyura, Eriphiidae) unveil genetic imprints of a late Pleistocene vicariant event across the Gibraltar Strait, erased by postglacial expansion and admixture among refugial lineages. *BMC Evol. Biol.* **2019**, *19*, 105. [CrossRef] [PubMed]

83. Petit, R.J.; Duminil, J.; Fineschi, S.; Hampe, A.; Salvini, D.; Vendramin, G.G. Invited Review: Comparative organization of chloroplast, mitochondrial and nuclear diversity in plant populations. *Mol. Ecol.* **2005**, *14*, 689–701. [CrossRef] [PubMed]

84. Yang, J.; Vázquez, L.; Feng, L.; Liu, Z.; Zhao, G. Climatic and Soil Factors Shape the Demographical History and Genetic Diversity of a Deciduous Oak (*Quercus liaotungensis*) in Northern China. *Front. Plant Sci.* **2018**, *9*, 1534. [CrossRef]

85. Ye, H.; Wang, Z.; Hou, H.; Wu, J.; Gao, Y.; Han, W.; Ru, W.; Sun, G.; Wang, Y. Localized environmental heterogeneity drives the population differentiation of two endangered and endemic *Opisthopappus* Shih species. *BMC Ecol. Evol.* **2021**, *21*, 56. [CrossRef] [PubMed]

86. Li, L.-F.; Cushman, S.A.; He, Y.-X.; Li, Y. Genome sequencing and population genomics modeling provide insights into the local adaptation of weeping forsythia. *Hortic. Res.* **2020**, *7*, 130. [CrossRef] [PubMed]

87. Guo, X.-D.; Wang, H.-F.; Bao, L.; Wang, T.-M.; Bai, W.-N.; Ye, J.-W.; Ge, J.-P. Evolutionary history of a widespread tree species Acer mono in East Asia. *Ecol. Evol.* **2014**, *4*, 4332–4345. [CrossRef]

88. Qi, X.-S.; Chen, C.; Comes, H.P.; Sakaguchi, S.; Liu, Y.-H.; Tanaka, N.; Sakio, H.; Qiu, Y.-X. Molecular data and ecological niche modelling reveal a highly dynamic evolutionary history of the East Asian Tertiary relict *Cercidiphyllum* (Cercidiphyllaceae). *New Phytol.* **2012**, *196*, 617–630. [CrossRef] [PubMed]

89. Zhao, P.; Zhou, H.-J.; Potter, D.; Hu, Y.-H.; Feng, X.-J.; Dang, M.; Feng, L.; Zulfiqar, S.; Liu, W.-Z.; Zhao, G.-F.; et al. Population genetics, phylogenomics and hybrid speciation of *Juglans* in China determined from whole chloroplast genomes, transcriptomes, and genotyping-by-sequencing (GBS). *Mol. Phylogenetics Evol.* **2018**, *126*, 250–265. [CrossRef] [PubMed]

90. Ye, J.-W.; Tian, B.; Li, D.-Z. Monsoon intensification in East Asia triggered the evolution of its flora. *Front. Plant Sci.* **2022**, *13*, 1046538. [CrossRef] [PubMed]

91. Song, Z.; Wan, S.; Colin, C.; Yu, Z.; Révillon, S.; Jin, H.; Zhang, J.; Zhao, D.; Shi, X.; Li, A. Paleoenvironmental evolution of South Asia and its link to Himalayan uplift and climatic change since the late Eocene. *Glob. Planet. Chang.* **2021**, *200*, 103459. [CrossRef]

92. Zhisheng, A.; Kutzbach, J.E.; Prell, W.L.; Porter, S.C. Evolution of Asian monsoons and phased uplift of the Himalaya–Tibetan plateau since Late Miocene times. *Nature* **2001**, *411*, 62–66. [CrossRef] [PubMed]

93. Wang, W.; Li, J.; Wang, J.; He, Z. Palynofloras from Pliocene Balouhe Formation and Pleistocene in Zhangqiu County, Shandong Province. *Acta Palaeontol. Sin.* **2002**, *41*, 72–76.

94. Ye, J.-W.; Zhang, Y.; Wang, X.-J. Phylogeographic breaks and the mechanisms of their formation in the Sino-Japanese floristic region. *Chin. J. Plant Ecol.* **2017**, *41*, 1003–1019.

95. Royden, L.H.; Burchfiel, B.C.; van der Hilst, R.D. The Geological Evolution of the Tibetan Plateau. *Science* **2008**, *321*, 1054–1058. [CrossRef] [PubMed]

96. Tian, S.; Kou, Y.; Zhang, Z.; Yuan, L.; Li, D.; López-Pujol, J.; Fan, D.; Zhang, Z. Phylogeography of *Eomecon chionantha* in subtropical China: The dual roles of the Nanling Mountains as a glacial refugium and a dispersal corridor. *BMC Evol. Biol.* **2018**, *18*, 20. [CrossRef] [PubMed]

97. Swenson, N.G.; Howard, D.J. Clustering of Contact Zones, Hybrid Zones, and Phylogeographic Breaks in North America. *Am. Nat.* **2005**, *166*, 581–591. [CrossRef] [PubMed]

98. Wu, C.; Zhang, X.; Ma, Y. The taihang and yan mountains rosemainly in quarteranary. *North China Earthq. Sci.* **1999**, *17*, 1–7.

99. Stefenon, V.M.; Klabunde, G.; Lemos, R.P.M.; Rogalski, M.; Nodari, R.O. Phylogeography of plastid DNA sequences suggests post-glacial southward demographic expansion and the existence of several glacial refugia for *Araucaria angustifolia*. *Sci. Rep.* **2019**, *9*, 2752. [CrossRef]

100. Zhao, C.; Wang, C.-B.; Ma, X.-G.; Liang, Q.-L.; He, X.-J. Phylogeographic analysis of a temperate-deciduous forest restricted plant (*Bupleurum longiradiatum* Turcz.) reveals two refuge areas in China with subsequent refugial isolation promoting speciation. *Mol. Phylogenet. Evol.* **2013**, *68*, 628–643. [CrossRef]